Crystallization and Microstructure in Quenched Slabs of Various Molecular Weight Polypropylenes

A. I. ISAYEV *and* B. F. CATIGNANI

Institute of Polymer Engineering
The University of Akron
Akron, Ohio 44325-0301

The purpose of this study was to accumulate material data for use in a simulation of morphology and crystallization in quenched slabs of isotactic polypropylenes (i-PP's). The molecular weight effect on the crystallization kinetics of various i-PP's were studied using isothermal and nonisothermal experiments. An experimental setup was constructed to measure the spherulite growth rate of i-PP's using isothermal and nonisothermal melt crystallization experiments. The molecular weight effect on spherulite growth rate of i-PP's was determined. Molecular weight effect on nuclei concentrations as a function of temperature was determined from growth and crystallization rate constants. The morphology and crystallization in quenched slabs of i-PP's were determined from experiments and compared to computer simulations. The molecular weight effect on the degree of crystallinity and morphology was determined for i-PP during quenching.

INTRODUCTION

A great deal of work (1–3) has been done on quiescent crystallization of i-PP's including effects of nucleating agent, molecular weight, isotacticity, catalyst system, and filler. Numerous isothermal and nonisothermal crystallization experiments are conducted in order to characterize the fast crystallization kinetics of i-PP's. Data obtained in these experiments should be useful for modeling of crystallinity and microstructure in various processing operations. In this case, extensive kinetic information is needed concerning rate of crystallization, rate of crystal growth, and nucleation density over a wide range of temperatures. However, the existing literature contains only bits of information in each of these areas. Therefore, the published data cannot be easily connected to become useful for microstructure modeling in processing.

A number of models are proposed to carry out simulation of the quiescent crystallization. These include models by Avrami (4–6), Tobin (7, 8), Nakamura (9), Ozawa (10), Hoffman-Lauritzen (11) and a recently proposed model by Schneider *et al.* based on a system of rate equations (12, 13). Crystallization modeling under flow conditions situation is a more complicated situation because of the complexity of the phenomena taking place during the crystallization process. Only in recent years has some advancement been made in this direction (14–17).

This paper deals with quiescent crystallization and describes our efforts to accumulate material data for carrying out a simulation of morphology and crystallinity in quenched slabs of i-PP's of various molecular weights. These efforts include measurements of isothermal and nonisothermal melt crystallization kinetics, spherulite growth rate, and a possibility of obtaining nuclei concentration.

EXPERIMENTAL

Materials and Methods of Investigation

Six grades of isotactic polypropylenes (i-PP) were used to study the molecular weight dependence on isothermal and nonisothermal crystallization. These grades include Profax 6823, 6723, 6523, Valtec HH444, HH441 and PPH910S supplied by Himont USA, Inc. PP6823, PP6723, and PP6523 are simply different melt flow grades of homopolymer polypropylene with a general purpose stabilization package. HH444 and HH441 are stabilized reactor spheres coated with a primary antioxidant and an acid neutralizing agent. PH910S is also a reactor sphere, but with minimal stabilization consisting of less than 100 ppm of a primary antioxidant. Material properties are given in *Table 1*.

Compression molding was used to obtain 1.5-mm-thick sheets of each grade. Approximately 5 mg of material was removed from these sheets and used for isothermal and nonisothermal crystallization study in nitrogen atmosphere, using a differential scanning calorimeter (DSC-7, Perkin Elmer). The sample was heated from room temperature to 200°C and annealed for 10 min. In isothermal experiments, the sample was

Table 1. Material Properties Provided by Himont.

Polymer	Lot #	MFI (dg/min) 230°C/2.16 kg	PI	M_w
PP6823	LK15077	0.51	3.9	670,000
PP6723	LK15026	0.92	3.9	557,000
PP623	BF37228	4.1	4.3	351,000
HH444	LK61306	73	4.3	144,000
HH441	LK06817	440	4.6	83,000
PH910S	LK06323	748	4.7	70,000

cooled at a rate of 50°C/min until the specified isothermal crystallization temperature was reached. In nonisothermal experiments, the sample was cooled to 50°C at various cooling rates 2.5, 5, 10, 20, and 40°C/min. More details on calibration and experimental procedures are given elsewhere (18–20).

The diameter of spherulites as a function of time during isothermal crystallization were measured using a special device built in our laboratory. A schematic of this device is shown in *Fig. 1*. The crystallization temperature was determined by an iron-constant thermocouple with a diameter of 75 microns. The thermocouple was inserted directly into the polymer sample. The sample was sandwiched between microscope slides at 200°C to obtain amorphous samples approximately 150 microns in thickness. The sample was then cooled at the rate of 50°C/min, using liquid nitrogen, until the desired isothermal crystallization temperature was reached. The growth rate was determined by measuring the size a spherulite as a function of time until the spherulite impinged. The slope of this line was the growth rate. Similar experiments were repeated for nonisothermal melt crystallization using cooling rates of 2.5, 5, 10, 20 and 40°C/min. Spherulites were measured over a narrow temperature range, typically 1°C to 7°C. The average of the temperature range for each experiment was taken to be the crystallization temperature.

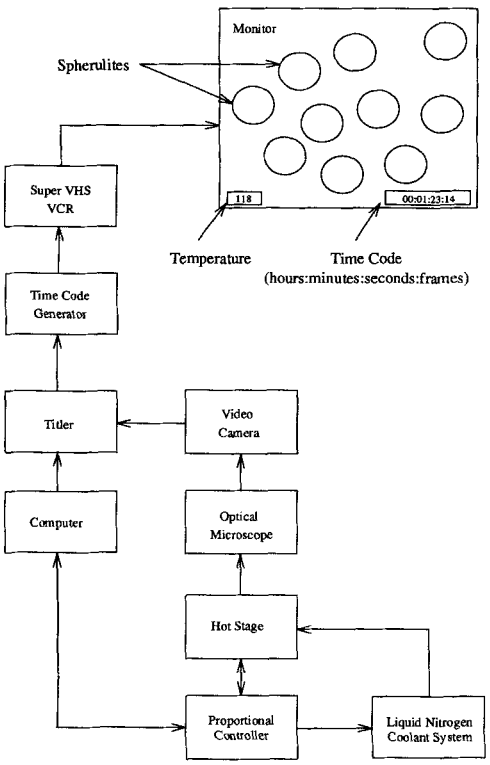

Fig. 1. Schematic of growth rate experiment.

Quenching experiments were carried out on square slabs 30 mm in width and 3.3 mm in thickness heated to 200°C and annealed for 10 min. Slabs were quenched from 200°C into water at 0°C and 25°C. Six layers were sliced from the wall to the core using a microtome. The gapwise distribution of degree of crystallinity in quenched slabs was measured using the DSC-7 by heating the sliced samples over temperature range of 60°C to 200°C with a 10°C/min scan rate. The relative crystallinity was calculated as a ratio of areas under melting peaks of the quenched sample and the fully crystallized sample obtained at a slow cooling (2.5°C/min). The heat of fusion was measured and the ultimate crystallinity was then determined as $X_\infty = \Delta H_f/\Delta H_c$, where ΔH_f is the area under the melting peak of the fully crystallized sample and ΔH_c is the latent heat of fusion of a perfect crystal of i-PP, which is 209 J/g according Van Krevelen (21). *Table 2* shows the melting point, T_m, heat of fusion, ΔH_f, and ultimate crystallinity, X_∞, of various i-PP's. The gapwise distribution of spherulite diameter in the quenched slab was also measured on microtome cuts of approximately 20 microns made along the thickness direction. Spherulite diameters were measured using a Leitz 12 Pol S Optical Microscope.

THEORETICAL

Quiescent Crystallization Kinetics

The overall crystallization kinetics was first formulated by Avrami (4–6); he assumed a fixed temperature independent value for the number of initially present nuclei per unit volume. The Avrami equation takes the form

$$\theta(t) = 1 - \exp[-k(T)t^n] \qquad (1)$$

where $\theta(t)$ is the fraction of crystallized material after some time, t at some isothermal crystallization temperature T, $k(T)$ is the isothermal rate constant, and n is the Avrami exponent.

The half time of conversion $t_{1/2}$, the time taken for 50% of the crystallization to occur, is derived from *Eq*

Table 2. Heat of Fusion, Ultimate Crystallinity, and Melting Point.

Polymer	H_f J/g	X_∞	T_m °C
PP6823	91	0.436	162
PP6723	96	0.460	162
PP623	111	0.529	162
HH444	122	0.583	162

1 and takes the form

$$t_{1/2} = \left(\frac{\ln 2}{k}\right)^{1/n} \tag{2}$$

which is inversely proportional to the overall rate of crystallization.

Since the conception of the Avrami model (4–6), numerous attempts (7–10, 22, 23) have been made to extend the theory to incorporate nonisothermal conditions. One such attempt was made by Nakamura *et al.* (9). The Nakamura theory is an extension of Avrami (4–6) and Evan's (24) theory of isothermal crystallization. On the basis of isokinetic conditions, the relative degree of crystallinity, at time t, $\theta(t)$, can be written as

$$\theta(t) = 1 - \exp\left[\left(\int_0^t K(T(t'))dt'\right)^n\right] \tag{3}$$

$K(T)$ is the nonisothermal crystallization rate constant. Differentiating *Eq 3* with respect to time, one obtains the differential form of the Nakamura equation.

$$\frac{d\theta}{dt} = nK(T)(1-\theta)[-\ln(1-\theta)]^{(n-1)/n} \tag{4}$$

A way of relating the isothermal rate constant and the nonisothermal rate constant is proposed by Nakamura *et al.* (9). This equation takes the form

$$K(T) = [k(T)]^{1/n} = \frac{(\ln 2)^{1/n}}{t_{1/2}} \tag{5}$$

According to Hoffman *et al.* (11) the overall rate of isothermal crystallization, $1/t_{1/2}$ may be expressed as

$$\left(\frac{1}{t_{1/2}}\right) = \left(\frac{1}{t_{1/2}}\right)_0 \exp\left(\frac{-U^*/R}{T - T_\infty}\right)\exp\left(\frac{-K_g}{T\Delta Tf}\right) \tag{6}$$

where

$$\Delta T = T_m^0 - T \text{ and } f = \frac{2T}{T + T_m^0}$$

R is the universal gas constant; T_m^0 is the equilibrium melting point; and f is a correction factor for the reduction in the latent heat of fusion, which is caused by decreasing temperatures. Thus expressed, the kinetic model has four parameters: $(1/t_{1/2})_0$ is a pre-exponential factor that includes all terms independent of temperature, U^* is the activation energy for the segmental jump rate, K_g is the nucleation exponent, and T_∞ is taken as the glass transition temperature minus 30°C.

Using *Eqs 5* and *6*, the temperature dependence of the nonisothermal rate constant may be expressed as

$$K(T) = (\ln 2)^{1/n}\left(\frac{1}{t_{1/2}}\right)_0 \exp\left(\frac{-U^*/R}{T - T_\infty}\right)\exp\left(\frac{-K_g}{T\Delta Tf}\right) \tag{7}$$

The Nakamura equation does not take into account an induction period for the crystallization process. The induction time can be determined by a method proposed by Sifleet *et al.* (25). The nonisothermal induction time can be obtained by a summation of isothermal induction times according to

$$\bar{t} = \int_0^{t_i} \frac{dt}{t_i(T)} = 1 \tag{8}$$

where t_i is the isothermal induction time, t_i is the nonisothermal induction time, and $\bar{t}$ is the induction time index. When the induction time index approaches unity, quiescent crystallization begins. For melt crystallization, the isothermal induction time is assumed to follow the Godovsky and Slonimsky (26) expression

$$t_i = t_m(T_m^0 - T)^{-a} \tag{9}$$

where t_m and a are material constants independent of temperature and can be determined using DSC.

GROWTH RATES AND NUCLEI CONCENTRATION

The radial growth rates can be determined by measuring the size of the spherulites as functions of time and temperature for isothermal and nonisothermal crystallization. The growth rate can be written as

$$G = \frac{dR}{dt} \tag{10}$$

where G is the radial growth rate and R is the radius of a growing spherulite at time t. The temperature dependence of the growth rate, $G(T)$, can be established by conducting numerous isothermal and nonisothermal experiments at various crystallization temperatures. According to Hoffman and Lauritzen (11), a kinetic description of the growth rate can be written as

$$G = G_0\exp\left(\frac{-U^*/R}{T - T_\infty}\right)\exp\left(\frac{-K_g}{T\Delta Tf}\right) \tag{11}$$

where G_0 is a pre-exponential factor containing quantities not strongly dependent on temperature.

The Avrami exponent is indicative of possible spherulite morphologies and nucleation mechanisms. For instantaneous nucleation, $n = 3$, all potential nucleation sites are already in their activated states. Therefore the growth rate, combined with crystallization rate constants, can be used to estimate the number of effective nuclei as a function of temperature. For spherulite growth with $n = 3$, the nuclei concentration, N, takes the form (14)

$$N(T) = \frac{3V_\infty k(T)}{4\pi G(T)^3} \tag{12}$$

where V_∞ is the maximum volume fraction of spherulites at $t \to \infty$.

Models of Impingement

Avrami (4–6) assumed a fixed temperature independent value for the number of initially present potential nuclei per unit volume. Taking impingement of growing spherulites into account and letting V be the transformed volume fraction, Avrami then assumed that the rate of change of V is proportional to the untransformed volume fraction, $(1 - V)$. Mandelkern (27) modified Avrami's work by incorporating incomplete crystallization, such that the rate of change of the transformed volume fraction is of the form:

$$dV = (1 - \theta)dV_e \tag{13}$$

where

$$\theta = \frac{V}{V_\infty} \tag{14}$$

and V_∞ is the largest possible transformed crystallized phase and V_e is the extended volume. Accordingly, Avrami's model of impingement, which neglects swallowing of nuclei, can be written as (12):

$$-\ln(1 - \theta) = \frac{\bar{N}}{V_\infty}\int_0^\tau \nu(\tau, z)e^{-z}dz \tag{15}$$

where $\bar{N}$ is the number of effective nuclei, $\nu(t, z)$ is the grain volume at non-dimensional time τ, which began growth at time z and takes the form:

$$\nu(\tau, z) = \frac{4\pi}{3}\left[\int_0^\tau \alpha\, dt'\right]^m \tag{16}$$

and

$$\alpha = \frac{G}{P} \tag{17}$$

with P being the probability of formation of growth nuclei per germ nucleus and unit time.

Tobin (7, 8) proposed that the transformed volume fraction be of the form:

$$V = (1 - \theta)V_e \tag{18}$$

such that V_e is determined by taking the swallowing of nuclei into account. Tobin's model of impingement can be written as (12):

$$\frac{\theta}{1 - \theta} = \frac{\bar{N}}{V_\infty}\int_0^\tau \nu(\tau, z)e^{-z}[1 - \theta(z)]dz \tag{19}$$

Transformation to a System of Rate Equations

According to Schneider *et al.* (12, 13), Avrami's model of impingement, *Eq 15*, can be evaluated by substituting *Eq 16* into *Eq 15* and differentiating $(m + 1)$ times with respect to τ, yielding a differential equation of order $(m + 1)$ for the dummy variable φ_1, where:

$$\varphi_0 = -\ln(1 - \theta),\ \theta = 1 - e^{-\varphi_0} \tag{20}$$

The system of rate equations can be written as follows:

$$\frac{L\partial\varphi_i}{G\partial t} = \varphi_{i+1} \quad (i = 0, 1, 2, \ldots, m - 1) \tag{20a}$$

$$\frac{1}{P}\frac{\partial\varphi_m}{\partial t} = 1 - \varphi_m \tag{20b}$$

subject to the initial conditions

$$\varphi_i = 0 \quad (i = 0, 1, 2, \ldots, m) \text{ at } t = 0 \tag{21}$$

where φ_0 is the unrestricted spherulite volume, φ_1, is the projection of this volume on a unit surface, φ_2 is its projection on unit line, and is the unrestricted number of activated nuclei per unit of volume according to Eder *et al.* (14). L is the average distance between nuclei and can be written as:

$$L = \left(\frac{3V_\infty}{4\pi m!\bar{N}}\right)^{1/m} \tag{22}$$

For instantaneous three-dimensional spherulitic growth, the constant L takes the form:

$$L = \left(\frac{V_\infty}{8\pi\bar{N}}\right)^{1/3} \tag{23}$$

Tobin's model of impingement, *Eq 19*, can be transformed by differentiating $(m + 2)$ times for the dummy variable, ψ_i, where:

$$\psi_0 = \frac{\theta}{(1 - \theta)},\ \theta = \frac{\psi_0}{(1 + \psi_0)} \tag{24}$$

The system of rate equation becomes:

$$\frac{L}{G}\frac{\partial\psi_i}{\partial t} = \psi_{i+1} \quad (i = 0, 1, 2, \ldots, m - 1) \tag{25a}$$

$$\frac{1}{P}\frac{\partial\psi_m}{\partial t} = \frac{1 - \psi_{m+1}}{1 + \psi_0} \tag{25b}$$

$$\frac{1}{P}\frac{\partial\psi_{m+1}}{\partial t} = 1 - \psi_{m+1} \tag{25c}$$

subject to the initial conditions

$$\psi_i = 0 \quad (i = 0, 1, 2, \ldots, m + 1) \text{ at } t = 0 \tag{26}$$

Limiting Cases

Under nonisothermal conditions, Schneider *et al.* (12, 13) proposed two limiting cases:

$$\text{Case I: } \frac{PL}{G} \to \infty, \quad \text{Case II: } \frac{PL}{G} \to 0 \tag{27}$$

For case II, the growth takes place much faster than nucleation, while in case I, activation of the nuclei takes place faster than the growth. For case I, this indicates immediate activation of all nuclei, which yields $\varphi_m = 1$ while φ_0 is determined from solving the

set of rate *Equations 20*. Introducing:

$$\varphi_{m-1} = \int_0^t \left(\frac{G}{L}\right) dt \tag{28}$$

as an independent variable, the system of rate equations can be integrated to obtain:

$$\varphi_0 = \left(\frac{1}{m!}\right) \varphi_{m-1}^m \tag{29}$$

or

$$\frac{\partial \Phi}{\partial t} = \frac{G}{L} \tag{30}$$

where

$$\Phi = (m!\varphi_0)^{1/m} \tag{31}$$

The same result is obtained for Tobin's with ψ_0 rather than φ_0. Therefore, a single rate equation, *Eq 30*, can describe both Avrami and Tobin's model of impingement for nonisothermal crystallization with a limiting case of $(PL/G) \rightarrow \infty$.

Using *Equations 28* and *29*, *Eq 20* can be written as:

$$\theta = 1 - \exp\left\{-\left(\frac{1}{m!}\right)\left(\int_0^t \left(\frac{G}{L}\right) dt\right)^m\right\} \tag{32}$$

which represents the degree of crystallinity for the Avrami model. The degree of crystallinity for Tobin's model, *Eq 24*, using the same substitutions becomes:

$$\theta = \frac{(1/m!)(\int_0^t (G/L)dt)^m}{1 + (1/m!)(\int_0^t (G/L)dt)^m} \tag{33}$$

CRYSTALLIZATION AND MORPHOLOGY IN QUENCHED SLABS

In order to predict the crystallinity distributions and morphology of i-PP slabs of finite thickness, an infinitely extended slab is considered. For this case a one-dimensional heat transfer problem arises in which the temperature varies only in the thickness direction. The one-dimensional equation of heat conduction, incorporating a heat of crystallization term, can be written as:

$$\rho C_p \frac{\partial T}{\partial t} = k \frac{\partial^2 T}{\partial z^2} + \rho \Delta H_c X_\infty \frac{\partial \theta}{\partial t} \tag{34}$$

where ρ, C_p, and k are the density, specific heat, and heat conductivity of the material, T is the temperature after time t at a distance z from the center of the sample in the thickness direction, and $\partial\theta/\partial t$ is the crystallization rate. The initial conditions are:

$$T(0, z) = T_i, \quad \theta(0, z) = 0 \quad \text{at } t = 0 \tag{35}$$

where T_i is the initial temperature of the molten polymer. The boundary conditions are

$$\frac{\partial T}{\partial t} = 0 \text{ at } z = 0 \text{ and}$$
$$-k\frac{\partial T}{\partial z} = h(T - T_q) \text{ or } \frac{\partial T}{\partial z} = -\frac{Bi}{H}(T - T_q) \text{ at } z = H \tag{36}$$

where $Bi = hH/k$ is the Biot number, H is the half thickness of the sample, T_q is the quench temperature, and h is the heat transfer coefficient between the sample and the quench medium.

The rate of crystallization in *Eq 34* varies depending on which crystallization model is used. For the Nakamura model, $\partial\theta/\partial t$ is given by *Eq 4*. For Avrami and Tobin's model, $\partial\theta/\partial t$ is determined by solving *Eqs 32* and *33* using the finite difference method.

In order to simulate and determine when crystallization began during the quenching process, the theory of nonisothermal induction times was incorporated into a FORTRAN program, which used 50 nodes across the half thickness H. Once the induction time reached unity, according to *Eq 8*, the crystallization process was assumed to begin. The effective number of nuclei $N(T)$ was then assumed to be instantaneous and was determined from *Eq 12*. The average distance between nuclei was determined by *Eq 23*, and this distance was assumed to be the average diameter of the spherulites at a particular node.

ACQUISITION OF PARAMETER VALUES FROM EXPERIMENTS

Nonisothermal Rate Constants

Nonisothermal crystallization experiments at various cooling rates were conducted using DSC. The degree of crystallinity as function of temperature was obtained. The master curve approach to crystallization kinetics was used to obtain master curves of shift factors as a function of temperature and crystallinity as a function of reduced time, ε, for all six i-PP's (18, 19). The reference half time, $(t_{1/2})_r$ was determined from the θ versus ε for each molecular weight i-PP. Using $(t_{1/2})_r$ and the corresponding shift factors for each molecular weight, i-PP the nonisothermal rate constant as a function of temperature was determined.

Isothermal and Nonisothermal Induction Times

Further, by fitting *Eq 8* to the nonisothermal induction times, the isothermal induction time parameters were obtained. These parameters are listed in *Table 3*. Using these parameters, the nonisothermal induction time for any thermal history can then be determined. *Figure 2* shows fitted curve and experimental data on the induction time versus cooling rate for PP6823.

Hoffman-Lauritzen Parameters

A nonlinear regression program incorporating the differential form of the Nakamura equation (*Eq 4*) with

Table 3. Isothermal Induction Time Parameters in Eq 8 Obtained by Fitting Eq 9.*

Polymer	$t_m \times 10^{18}$ (sK^6)	a
PP6823	17.1	10.0
PP6723	4.39	10.0
HH6523	5.99	10.0
HH444	3.04	10.0
HH441	6.52	10.1
PH910S	4.20	10.1

* T_m^0 = 172°C was taken from Van Krevelen (21) and used in fitting.

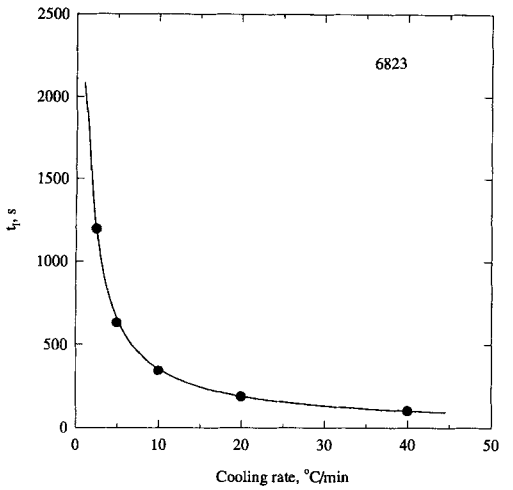

Fig. 2. Nonisothermal induction time as a function of cooling rate for PP6823. Symbols represent experimental data while solid line represents nonlinear regression.

$n = 3$ was used to determine the Hoffman-Lauritzen parameters, K_g and $(1/t_{1/2})_0$. In *Eq 4*, $K(T)$ is described by *Eq 7* and incorporates the Hoffman-Lauritzen parameters. *Equation 4* can be solved using the initial condition that $\theta = 0$, after the induction time index for quiescent crystallization reaches one. Values for the degree of crystallinity, as a function of temperature, used in this fitting, are determined from numerous nonisothermal DSC experiments. *Table 4* lists the Hoffman-Lauritzen parameters. The results of this fitting along with experimental data on relative crystallinity versus temperature at various cooling rates are shown in *Fig. 3* for PP6823. *Table 4* indicates a slight decreasing K_g with decreasing molecular weight. At the same time, the melting point of all the i-PP samples measured by the DSC at 10°C/min heating rate was found to be 162°C and independent of molecular weight, as indicated in *Table 2*. Therefore, the significance of the dependence of the K_g parameter (*Table 4*) on molecular weight is presently unclear.

Table 4. Hoffman-Lauritzen Parameters Fitted to Eq 7.

Polymer	$(1/t_{1/2})_0 \times 10^7$ (s^{-1})	$K_g \times 10^5$ (°K^2)
PP6823	15.28	3.81
PP6723	38.58	3.93
PP6523	54.95	3.99
HH444	6.84	3.45
HH441	3.14	3.30
PH910S	2.46	3.28

The crystallization kinetics of six molecular weight i-PP's were plotted together in *Fig. 4*. When the Valtec grades, HH444, HH441, and PH910S, were compared with the Profax grades, PP6823, PP6723, and PP6523, it was obvious that the crystallization rate did not increase as molecular weight decreased. This phenomenon was not anticipated and could be due to the fact that the Valtec grades are reactor spheres and use a different stabilization package than the homopolymer Profax grades. Additionally, different catalyst systems were possibly employed, which give rise to different crystallization kinetics, as noted by Avella *et al.* (28). However, it was noteworthy that the overall crystallization kinetics of the Valtec grades were consistent with each other. The shapes of the curves were consistent over a large temperature range and the maximum rate of crystallization occurred at 70°C, for HH444, HH441, and PH910S. This maximum was approximately midway between the glass transition temperature and the equilibrium melting point.

Growth Rates

Figure 5 represents measured spherulite diameters versus time for various isothermal crystallization temperatures for PP6823. The slopes of these lines represent the growth rate at a particular temperature. For all four i-PP's, higher crystallization temperatures correspond to longer crystallization times and subsequently slower growth velocities.

Figure 6 depicts typical measured diameters versus crystallization time for various nonisothermal experiments for PP6823. Each plot represents a single spherulite that was measured along a particular cooling curve. For all four i-PP's faster cooling rates correspond to faster growth rates. As the cooling rate increased, the induction time and the temperature of crystallization both decreased. Thus, at faster cooling rates, lower crystallization temperatures were obtained, which correspond to faster growth rates.

Figure 7 represents the growth rates for PP6823 obtained from isothermal, *Fig. 5*, and nonisothermal, *Fig. 6*, growth rate experiments for each i-PP; the growth rates overlap each other with a smooth transition from isothermal to nonisothermal data. This indicates that both isothermal and nonisothermal experiments can be used to determine growth rates. For each i-PP, the growth rate increased as the crystallization temperature decreased. The result was consistent with phenomena reported by Avella *et al.* (29), Tai *et al.* (30), Huang *et al.* (31), and Ding and Spruiell (32).

Figure 8 depicts the growth rates for all four i-PP's. Combining PP6823, PP6723, and PP6523, the growth rate depends only on temperature and was not a function of molecular weight. Eder *et al.* (14) compared PP growth rates of Padden and Keith (33), Falkai (34), and Lovinger *et al.* (35) with their own. Eder *et al.* (14) noted that there was a lack of dependence of these

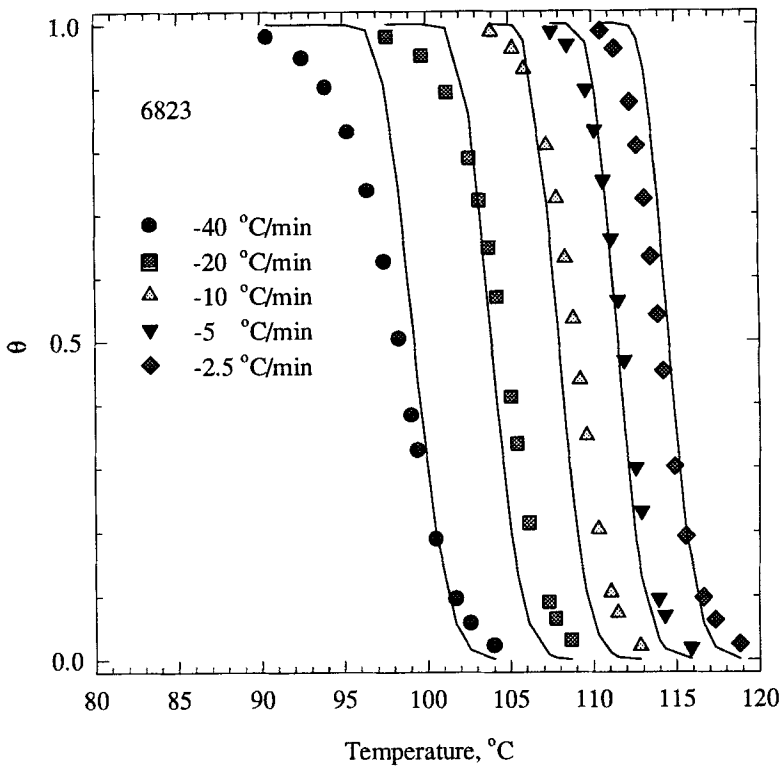

Fig. 3. Relative crystallinity versus temperature during nonisothermal crystallization of PP6823 at various cooling rates. Symbols represent experimental data while solid lines indicate nonlinear regression.

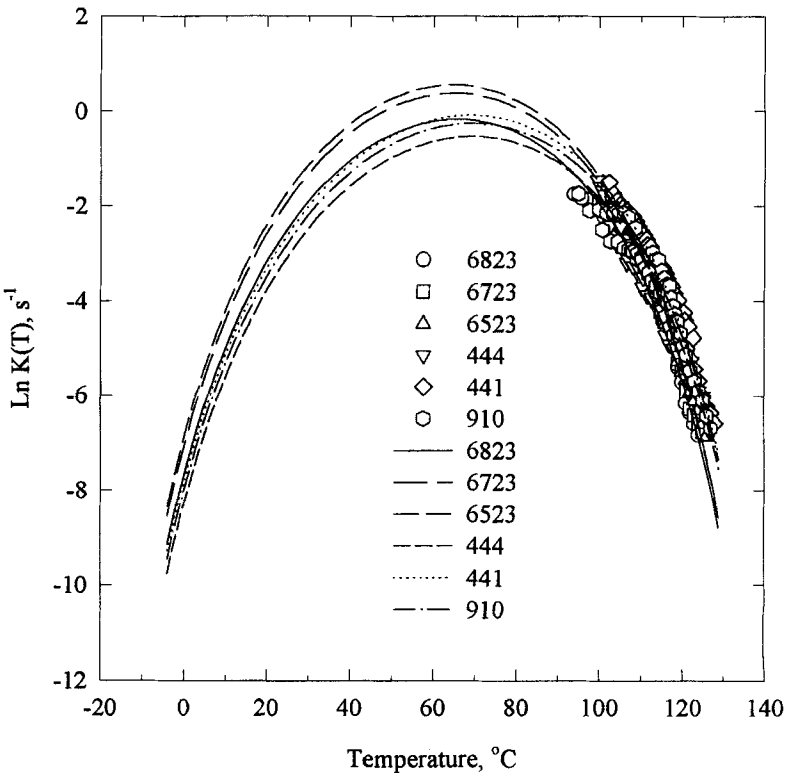

Fig. 4. Nonisothermal crystallization rate constants for various i-PP's. Symbols represent data while lines represent nonlinear fits to the Hoffman-Lauritzen equation (Eq 7).

growth rates on the molecular weight. These results are consistent with Magil (36, 37) in that above a certain maximum molar mass, the linear growth speed of spherulites is independent of the molar mass. This lack of dependence on molecular weight was also observed by Pospisil and Rybnikar (38). They investigated the crystallization behavior of various-molecular-weight PP's prepared by peroxide melt degradation. They noted that the spherulite growth rate did not depend on the molecular weight.

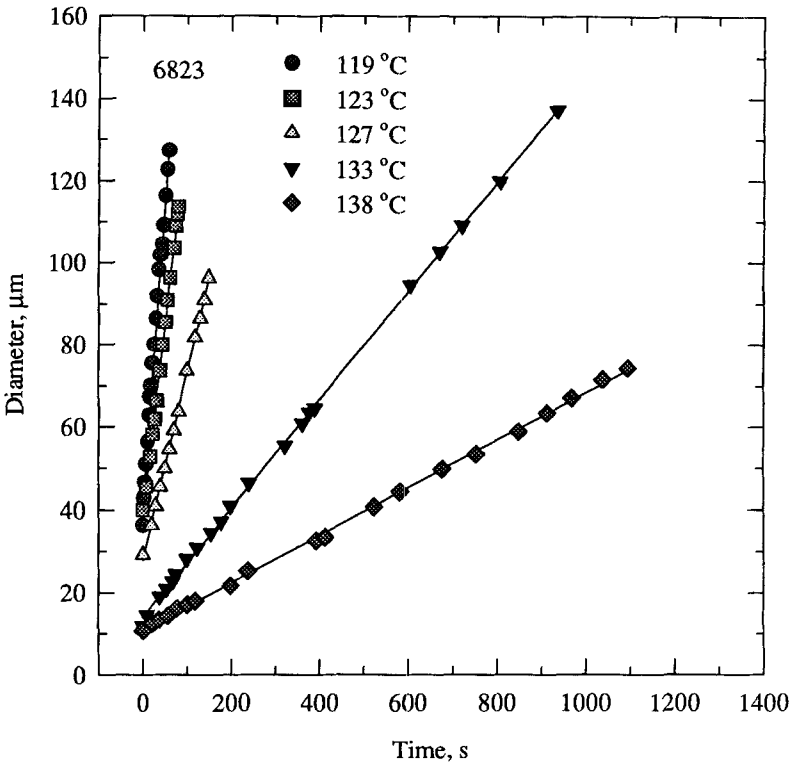

Fig. 5. Typical linear radial growth of PP6823 spherulites at various isothermal crystallization temperatures.

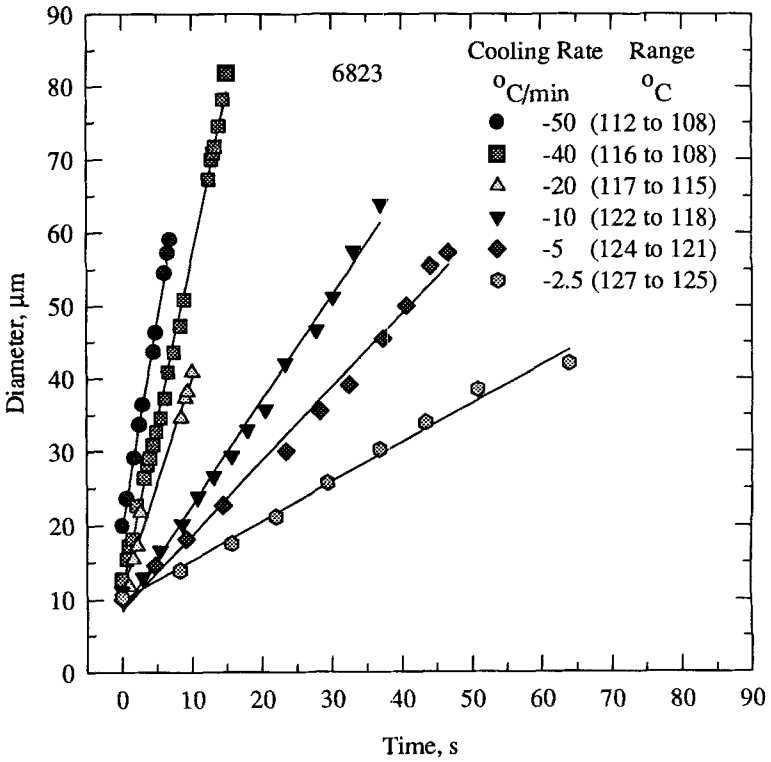

Fig. 6. Typical radial growth of PP6823 spherulites at various cooling rates and the temperature range at which the spherulites were measured.

For all four i-PP's, HH444 appears to have a faster growth rate than that of PP6823, PP6723, and PP6523, which indicates a growth rate molecular weight dependence. It appears that the growth rate of i-PP becomes molecular weight dependent somewhere between 351,000 and 144,000 g/mol or that the difference between Profax and Valtec grades affected the growth rate.

Ding and Spruiell (32) conducted nonisothermal growth rate experiments with cooling rates of 2500°C/

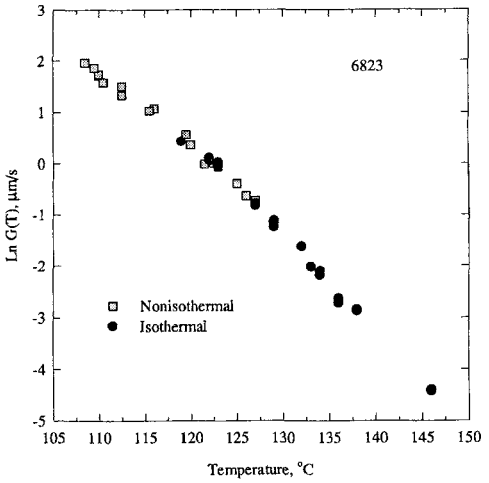

Fig. 7. Spherulite growth rates for PP6823 as a function of crystallization temperature.

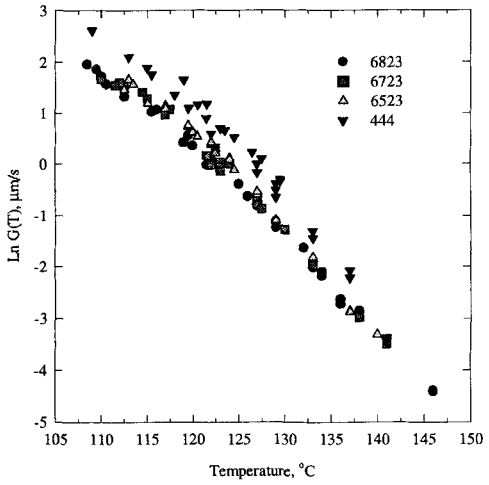

Fig. 8. Spherulite growth rate as a function of crystallization temperature for various molecular weight i-PP's.

min on a i-PP resin having a MFI of 18, M_w of 226,200 g/mol, and polydispersity of 5.87. *Figure 9* represents growth data obtained from Ding and Spruiell combined with growth rates obtained for PP6823, PP6723, and PP6523. The line represents a nonlinear curve fit to the Hoffman-Lauritzen growth rate equation (*Eq 11*) with fitted parameters listed in *Table 5*. The Hoffman-Lauritzen growth rate equation fits the data rather well and enables the prediction of the growth rate over a large temperature range otherwise unattainable through experiments. The maximum predicted growth rate occurred at 80°C, which was approximately midway between T_g and T_m. It should be noted that K_g parameters in *Table 4* determined from the DSC measurements differ from those in *Table 5* determined from the growth rate experiments. Possibly, these differences are due to the fact that the DSC measurements are based on enthalpic changes during crystallization, while the growth rate measurements are based on volume filling. Interestingly enough, the growth rate data depicted in *Fig. 9* do not exhibit

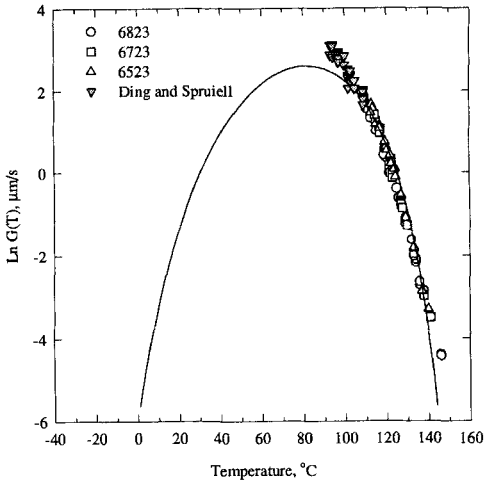

Fig. 9. Spherulite growth rate as a function of temperature for various molecular weight i-PP's. Symbols represent data while line indicates a nonlinear fit to the Hoffman-Lauritzen growth equation (Eq 11).

Table 5. Hoffman-Lauritzen Growth Rate Parameters Fitted to Eq 11.

Polymer	$G_0 \times 10^6$ $\mu m\ s^{-1}$	$K_g \times 10^5$ $(°K^2)$
PP6823, PP6723, PP6523	3.655	1.899
HH444	5.124	1.875

various regimes of crystallization as observed by Clark and Hoffman (39). However, the temperature range of the present growth rate measurements falls within Regime III of crystallization of i-PP given by them.

Nuclei concentrations were calculated for PP6823, PP6723, and PP6523, using *Eq 12* with curve fitted equations for the rate constant and the growth rate. Since the growth rate was independent of molecular weight, the nuclei concentration was directly proportional to the rate constant, which was observed to increase as molecular weight decreased. Thus, the effective number of nuclei for a particular crystallization temperature should increase as molecular weight decreases. This anticipated phenomenon, represented in *Fig. 10*, clearly shows an increased number of effective nuclei as molecular weight decreased. This result corresponds to data reported by Fillion *et al.* (40).

COMPARISON OF THEORY WITH EXPERIMENT

Crystallinity and Spherulite Diameters in Quenched Slabs

Figure 11 depicts the gapwise distribution of relative crystallinity in slab for PP6823, PP6723, PP6523, quenched from 200°C into water 25°C and for HH444 quenched from 170°C into water at 25°C. Similar data were obtained for slabs quenched to 0°C. For each i-PP, the relative crystallinity was somewhat lower for samples quenched to 0°C in comparison with those quenched to 25°C. This was related to the cooling rate experienced by the slab. Slabs quenched to 0°C expe-

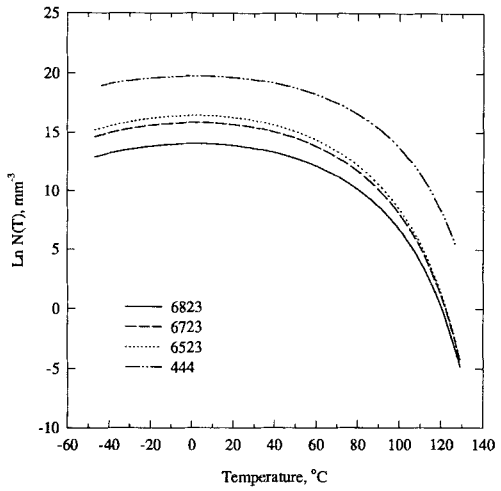

Fig. 10. Nuclei concentration as a function of temperature for various molecular weight i-PP's.

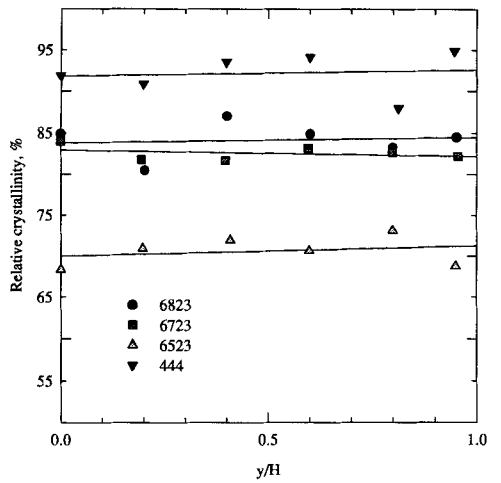

Fig. 11. Gapwise distribution of relative crystallinity in slabs of PP6823, PP6723, PP6523 quenched from 200°C to 25°C and HH444 quenched from 170°C to 25°C. Symbols represent data while lines represent first order regression.

rienced a greater cooling rate and had less time to crystallize.

It was also observed that the crystallinity distribution was rather flat, indicating that the entire slab crystallized to the same extent. This result was not anticipated, and a distribution of increasing degree of crystallinity from the wall to core was expected. Possible explanations as to why a flat profile was obtained could be related to the cooling rate. If the core crystallized at a slower rate, it takes a greater amount of time to pull heat away from the center by simple heat conduction. With a slower cooling rate, a greater amount of time is allowed for the crystallization process. Thus, a greater degree of crystallinity would be observed. Since this did not occur, it was likely that the core does not have a significantly slower cooling rate than the rest of the slab. Another possible explanation could be attributed to the rates of crystallization across the entire slab thickness. If the rate of crystallization was appreciable across the entire slab then crystallization would occur to its fullest extent in the core and at the wall.

The degree of crystallinity was simulated for each quenching condition using Nakamura, Avrami, and Tobin's theory of crystallization. All simulated results produced 100% relative crystallinity for each grade, under both quenching temperatures, across the entire thickness. The reason for this was quite simple. All three models are derived using geometric considerations. That is, the degree of crystallinity is considered to be the degree of space covering. In actuality, this is not the case. The microstructure was composed entirely of spherulites, but the measured degree of crystallinity, *Fig. 11*, shows values less than 100%. It is well known that spherulites are composed of amorphous and crystalline regions. No geometric model, Nakamura's, Avrami's, or Tobin's, has a way of predicting which regions of the spherulite were amorphous. Therefore, the degree of space covering, caused by the growth of spherulites, was considered to be a 100% crystalline entity for each model, which in fact was not the case.

With the exception of HH444, for each quench temperature the relative degree of crystallinity increased as molecular weight increased. Even though lower molecular weight grades of i-PP have faster crystallization rates, the relative extent to which they crystallized decreased as molecular weight decreased. It was also noted that PP6823 and PP6723 have rather similar values for the degree of crystallinity, while PP6523 was about 15% lower for both quench temperatures. The discrepancies between HH444 and PP6823, PP6723, and PP6523 could be attributed to the fact that the Valtec grades are reactor spheres and use a different stabilization package than the homopolymer Profax grades. Additionally, different catalyst systems could have been employed. Avella *et al.* (28) noted that different catalyst systems produced i-PP's that differed not only in stereoregularity, in this case isotactic, but also in atactic content. Avella *et al.* (28) also noted the different crystallization rates were obtained for i-PP's that used different catalyst systems. Any of these unknown factors could be attributed to the differences between the Profax and Valtec grades.

Figures 12, 13, and *14* represent, respectively, the gapwise distribution of spherulite diameters for PP6823, PP6723, and PP6523 quenched from 200°C to 0°C and 25°C. Generally greater diameters were obtained for slabs quenched to 25°C. The slabs quenched to 25°C experienced a slower cooling rate. A slab cooled at slower rates experienced a greater induction time, which corresponds to a start of crystallization, and number of effective nuclei. Thus, different numbers of effective nuclei and maximum spherulite diameters were obtained.

Another possible explanation includes the swallowing or disappearance of potential nuclei as the crystallization process proceeds. If fewer nuclei are available, then the spherulites can grow to greater dimensions than otherwise expected from an initial

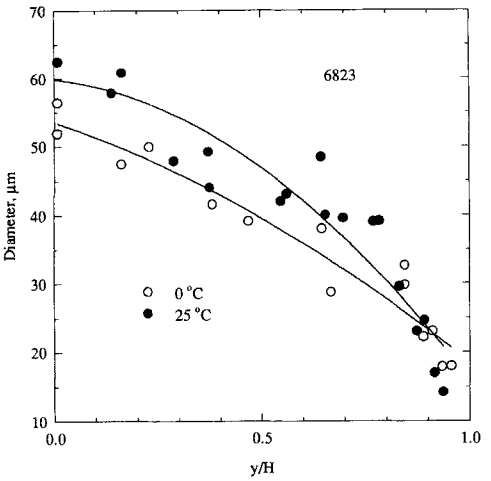

Fig. 12. Gapwise distribution of spherulite diameters in PP6823 slabs quenched from 200°C to 0°C and 25°C. Symbols represent data while line represent second order regression.

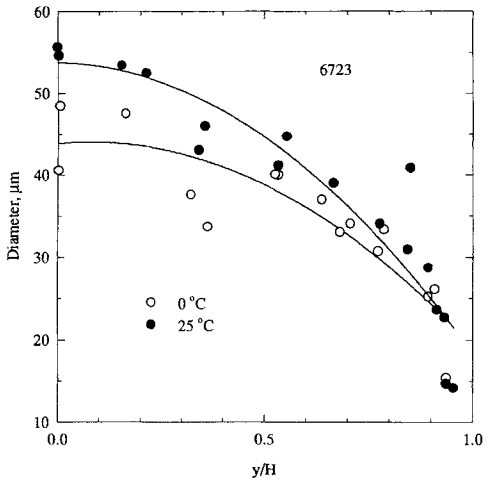

Fig. 13. Gapwise distribution of spherulite diameters in PP6723 slabs quenched from 200°C to 0°C and 25°C. Symbols represent data while lines represent second order regression.

estimate of nuclei. Swallowing of potential nuclei violates the premise of instantaneous nucleation. If all potential nuclei begin growing at the same time, then it is impossible for any nuclei to be swallowed. Instantaneous nucleation was assumed, but it was possible that mixed nucleation existed. Evidence for mixed nucleation was observed while accumulating data for the growth rate experiment. Once crystallization began, a finite number of nuclei were activated at a particular crystallization temperature. As the crystallization process proceeded, new nuclei would appear and begin to grow. These new spherulites had smaller final diameters than those first initiated. The appearance of additional nuclei was an indication of sporadic nucleation occurring after a finite number of initial nuclei began to grow. If mixed nucleation occurred, it was impossible with the models used in this simulation to determine how many nuclei were actually present during the crystallization process.

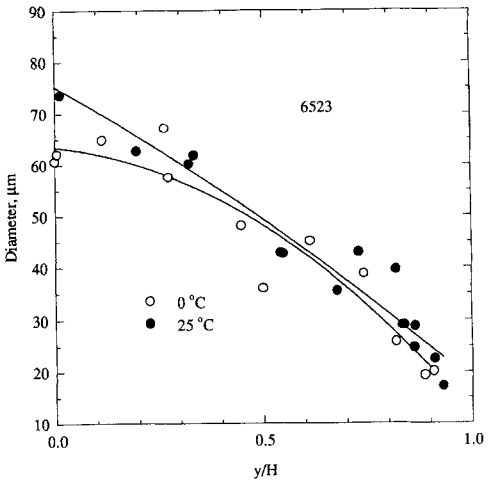

Fig. 14. Gapwise distribution of spherulite diameters in PP6523 slabs quenched from 200°C to 0°C and 25°C. Symbols represent data while lines represent second order regression.

Figures 15, 16, and *17* represent, respectively, the gapwise distribution of predicted and measured spherulite diameters for PP6823, PP6723, and PP6523 quenched from 200°C to 25°C. For each condition, the Nakamura, Avrami, and Tobin models of crystallization were used, in which three values for the heat transfer coefficient were assumed: 62.5, 125, 250 J/s m^2 °K. The Nakamura model predicted the greatest spherulite diameter while the Avrami model was second and the Tobin model predicted the smallest of the three. A greater heat transfer coefficient, for all three models, predicted smaller spherulite diameters. For higher heat transfer coefficients, the polymer was cooled at a faster rate, which enabled a greater degree of super cooling for which a lower crystallization temperature was predicted. A lower crystallization temperature corresponds to a greater number of effective nuclei, which means the spherulites will impinge before they can grow to larger dimensions. Sifleet *et al.* (25) and Chan and Isayev (20) noted that the heat transfer coefficient affects the rate of heat loss and caused different cooling rates.

For PP6823 quenched 25°C, *Fig. 15*, h = 250 J/(s m^2 °K) near the wall best predicts the spherulite diameter, while at intermediate distances, h = 125 J/(s m^2 °K) fits the data, and for the core, h = 62.5 J/(s m^2 °K). Similar results were obtained for PP6723 and PP6523. This phenomenon could indicate that the heat transfer coefficient was not a constant but rather a variable as the cooling process proceeded. Another explanation was that the model used for predicting spherulite diameters was too simplistic and can give only approximate values. The simplicity of the present model is due to the fact that it is based on the instantaneous nucleation while in reality the nucleation process is sporadic. In addition, the present calculations were carried out using constant thermal properties based on the PP melt. A further work is in progress to incorporate variation of thermal properties with temperature into simulation.

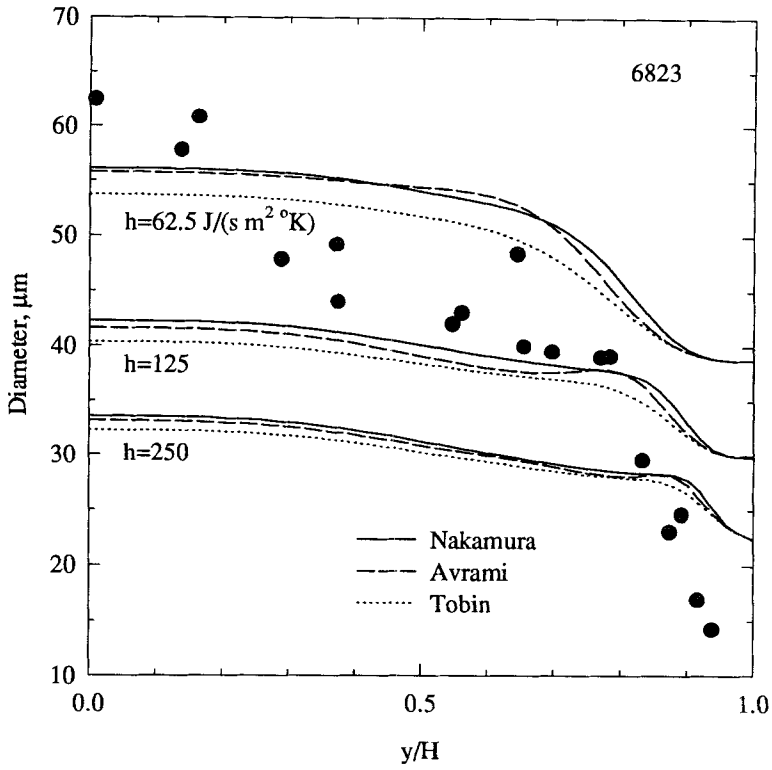

Fig. 15. Gapwise distribution of predicted (lines) and measured (symbols) spherulite diameters in a slab of PP6823 of thickness 3.3 mm quenched from 200°C to 25°C. Predictions were based on various heat transfer coefficients, h.

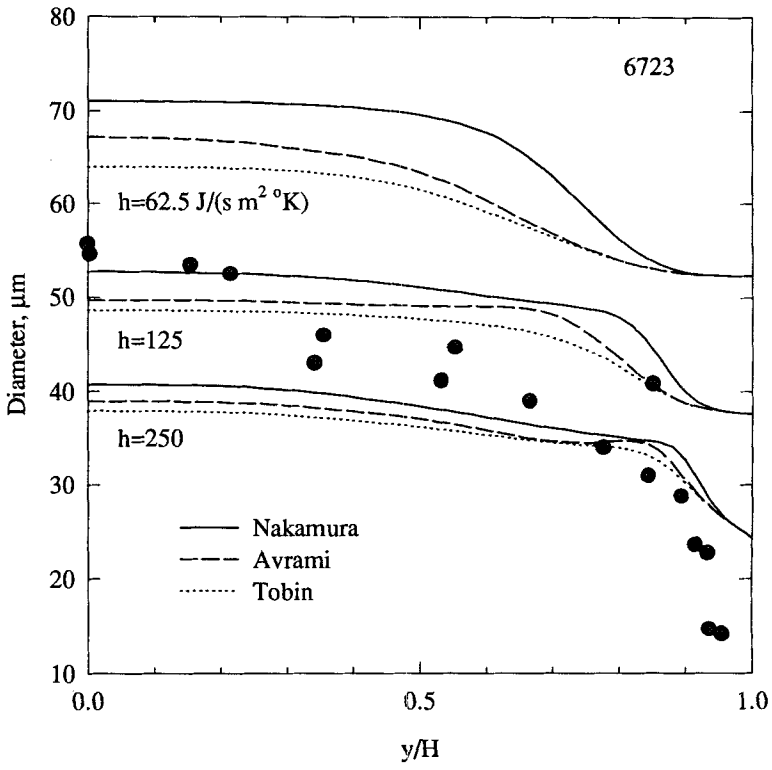

Fig. 16. Gapwise distribution of predicted (lines) and measured (symbols) spherulite diameters in a slab of PP6723 of thickness 3.3 mm quenched from 200°C to 25°C. Predictions were based on various heat transfer coefficients, h.

From *Figs. 15, 16,* and *17* it was observed that the predicted increase in spherulite diameter from the wall to the core was not always a smooth transition. A small peak and valley was observed in simulated data. This fluctuation was due to the temperature at which the polymer crystallized. The same type of peak and valley in the predicted crystallization temperature was observed as depicted in *Fig. 18* for the gapwise distribution of the crystallization temperature for PP6823. The changing crystallization temperature was due to

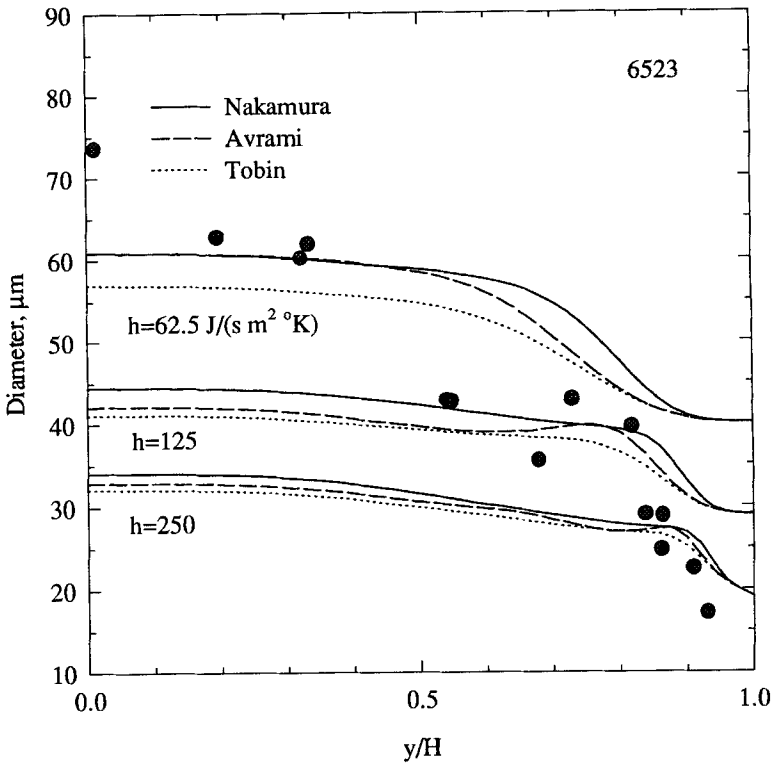

Fig. 17. Gapwise distribution of predicted (lines) and measured (symbols) spherulite diameters in a slab of PP6523 of thickness 3.3 mm quenched from 200°C to 25°C. Predictions were based on various heat transfer coefficients, h.

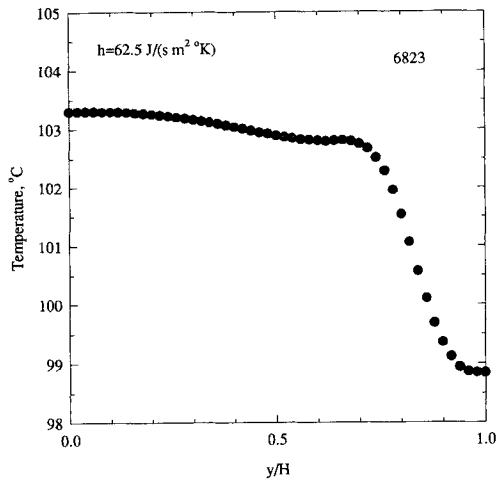

Fig. 18. Gapwise distribution of predicted crystallization temperatures in a slab of PP6823 of thickness 3.3 mm quenched from 200°C to 0°C. Prediction based on the Avrami model with a heat transfer coefficient of 62.5 J/(s m^2 °K).

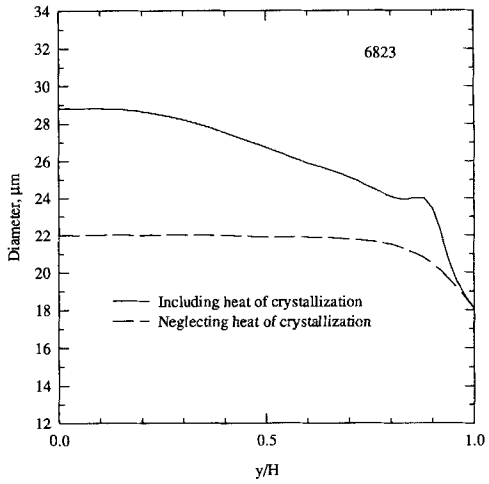

Fig. 19. Gapwise distribution of predicted spherulite diameters in a slab of PP6823 of thickness 3.3 mm quenched from 200°C to 0°C based on the Avrami model with h = 250 J/(sm^2 °K). Lines indicate predictions with and without a source term for the heat of crystallization.

the evolved heat of crystallization and was observed to be approximately 1°C. This slight change in crystallization temperature produces a change in simulated spherulite diameter of approximately 2 to 3 microns.

Figure 19 represents gapwise distribution of predicted spherulite diameters, based on the Avrami model with h = 250 J/(s m^2 °K), with and without a source term for the heat of crystallization. It is obvious that the heat of crystallization plays a major role in calculating the final spherulitic diameter. Omitting the heat of crystallization produces final spherulite diameters that are smaller. Neglecting the heat of crystallization allows the slab to cool at a faster rate. Faster cooling rates lowered the crystallization temperature, which in turn produced a large number of activated nuclei; see *Fig. 10.*

CONCLUSION

A method was developed to simulate microstructure. The predicted microstructure was compared with experimental results. This was the first time such

an attempt was made. For i-PP's, as the molecular weight decreased, the heat of crystallization increased, and a greater ultimate degree of crystallinity was obtained. For each i-PP, the relative crystallinity was lower for samples quenched at 0°C than for those quenched to 25°C. It was also observed that the gapwise crystallinity distribution was rather flat, indicating that the entire slab crystallized to the same extent. Using the theory of nonisothermal induction times, the number of crystallizing nuclei was determined for the simulation. This was the first time such an approach was used. The degree of crystallinity was simulated for each quenching condition using Nakamura's, Avrami's, and Tobin's theories of crystallization. All simulated results produced 100% relative crystallinity for each grade, under both quenching temperatures, across the entire thickness. Experimental data indicated that the relative degree of crystallinity for Profax samples increased as molecular weight increased. For all i-PP's, greater spherulite diameters were obtained for slabs quenched to 25°C. Maximum diameters of 63, 55, and 75 microns at 25°C were obtained for PP6823, PP6723, and PP6523, respectively. For PP6823, PP6723, and PP6523, quenched 0°C and 25°C, the Nakamura model predicted the greatest spherulite diameter while the Avrami model was second and the Tobin model predicted the smallest of the three. A greater heat transfer coefficient, for all three models, predicted smaller spherulite diameters. A transition of heat transfer coefficients with larger values fitting the data near the wall and smaller values fitting the data near the core was hypothesized for PP6823, PP6723, and PP6523. This phenomenon could indicate that the heat transfer coefficient was not a constant, but rather a variable during the cooling process. Another explanation was that the model using for predicting spherulite diameters was too simplistic and can give only approximate values.

ACKNOWLEDGMENTS

Financial support by a fellowship from the Dow Chemical Company is gratefully acknowledged. The authors wish to thank Mr. Ronald Mase, Mr. Carl Kissinger, and Mr. Tom Miner for their help in building the equipment used to obtain the growth rate data. Special thanks are due to Dr. Adam Galambos of Himont U.S.A., Inc., for supplying the polypropylenes used in this study.

REFERENCES

1. B. Wunderlich, *Crystal Nucleation, Growth, Annealing*, Academic Press, New York (1976).
2. L. Mandelkern, *Crystallization of Polymers*, McGraw-Hill, New York (1964).
3. L. Mandelkern, "Crystallization and Melting of Polymers," in G. Allen, ed., *Comprehensive Polymer Science*, Vol. 2, Pergamon Press, Oxford, England (1989).
4. M. Avrami, *J. Chem. Phys.*, **7,** 1103 (1939).
5. M. Avrami, *J. Chem. Phys.*, **8,** 812 (1940).
6. M. Avrami, *J. Chem. Phys.*, **9,** 1977 (1941).
7. M. C. Tobin, *J. Polym. Sci. Poly. Phys. Ed.*, **12,** 399 (1974).
8. M. C. Tobin, *J. Polym. Sci. Poly. Phys. Ed.*, **14,** 2253 (1976).
9. K. Nakamura, K. Katayama, and T. Amano, *J. Appl. Polym. Sci.*, **17,** 1031 (1975).
10. T. Ozawa, *Polymer*, **12,** 150 (1971).
11. J. D. Hoffman, G. W. Davis, and S. I. Lauritzen, in *Treatise on Solid State Chemistry*, Vol. 3, Ch. 7, N. B. Hannay, ed., Plenum, New York (1976).
12. W. Schneider, A. Koppl, and J. Berger, *Intern. Polym. Proc.*, **2,** 151 (1988).
13. W. Schneider, J. Berger, and A. Koppl, *Proc. First International Conference on Transport Phenomena in Processing* (March 22–26, 1992).
14. G. Eder, H. Janeschitz-Kriegl, and S. Liedauer, *Prog. Polym. Sci.*, **15,** 629 (1990).
15. G. Eder, H. Janeschitz-Kriegl, in *Material Science and Technology*, Vol. 18, H. E. H. Meijer, ed., Verlag Chemie, Weinheim, (1995).
16. A. I. Isayev, T. W. Chan, K. Shimojo, and M. Gmerek, *J. Appl. Polym. Sci.*, **55,** 807 (1995).
17. A. I. Isayev, T. W. Chan, M. Gmerek, and K. Shimojo, *J. Appl. Polym. Sci.*, **55,** 821 (1995).
18. T. W. Chan, G. D. Shyu, and A. I. Isayev, *Polym. Eng. Sci.*, **35,** 733 (1995).
19. T. W. Chan, L. Guo, and A. I. Isayev, *SPE ANTEC Tech. Papers*, **41,** 1476 (1995).
20. T. W. Chan, and A. I. Isayev, *Polym. Eng. Sci.*, **34,** 461 (1994).
21. D. W. Van Krevelen, *Properties of Polymers*, 3rd Ed., Elsevier, Amsterdam (1990).
22. A. Ya. Malkin, V. P. Beghishev, I. A. Keapin, and Z. S. Andrianova, *Polym. Eng. Sci.*, **24,** 1396 (1984).
23. A. Ya. Malkin, V. P. Beghishev, I. A. Keapin, and Z. S. Andrianova, *Polym. Eng. Sci.*, **24,** 1402 (1984).
24. U. R. Evans, *Trans. Faraday Soc.*, **41,** 365 (1945).
25. W. L. Sifleet, N. Dinos, and J. R. Collier, *Polym. Eng. Sci.*, **13,** 10 (1973).
26. Y. K. Godovsky and G. L. Slonimsky, *J. Polym. Sci., Phys. Ed.*, **12,** 1053 (1974).
27. L. Mandelkern, N. L. Jain, and H. Kim, *J. Polym. Sci.*, **A-2, 6,** 165 (1968).
28. M. Avella, E. Martuscelli, and M. Pracella, *J. Thermal Anal.*, **28,** 237 (1983).
29. M. Avella, E. Martuscelli, C. Sellitti, and E. Garagnani, *J. Mater. Sci.*, **22,** 3185 (1987).
30. H. J. Tai, W. Y. Chiu, L. W. Chen, and L. H. Chu, *J. Appl. Polym. Sci.*, **42,** 311 (1991).
31. T. Huang, A. D. Rey, and M. R. Kamal, *Polymer*, **35,** 5434 (1994).
32. Z. Ding and J. E. Spruiell, *SPE ANTEC Tech. Papers*, **40,** 1485 (1994).
33. F. J. Padden, Jr., and H. D. Keith, *J. Appl. Phys.*, **30,** 1485 (1959).
34. B. Falkai, *Macromol. Chem.*, **41,** 86 (1960).
35. A. J. Lovinger, J. O. Chua, and C. C. Gryte, *J. Polym. Sci., Phys. Ed.*, **15,** 641 (1977).
36. H. J. Magil, *J. Appl. Phys.*, **35,** 3249 (1964).
37. H. J. Magil, *J. Polym. Sci.*, **A-2, 5,** 89 (1967).
38. L. Pospisil and F. Rybnikar, *Polymer*, **31,** 476 (1990).
39. E. J. Clark and J. D. Hoffman, *Macromolecules*, **17,** 878 (1984).
40. B. Fillion, B. Lotz, A. Thierry, and J. C. Wittmann, *J. Polym. Sci., Phys. Ed.*, **31,** 1395 (1993).